The Performance-Determining Role of Lewis Bases in Dye-Sensitized Solar Cells Employing Copper-Bisphenanthroline Redox Mediators

*Sebastian O. Fürer, Rebecca A. Milhuisen, Muhammad K. Kashif, Sonia R. Raga, Shravan S. Acharya, Craig Forsyth, Maning Liu, Laszlo Frazer, Noel W. Duffy, C. André Ohlin, Alison M. Funston, Yasuhiro Tachibana, and Udo Bach**

Copper redox mediators have enabled open-circuit voltages (V_{OC}) of over 1.0 V in dye-sensitized solar cells (DSCs) and have helped to establish DSCs as the most promising solar cell technology in low-light conditions. The addition of additives such as 4-*tert*-butylpyridine (tBP) to these electrolytes has helped in achieving high solar cell performances. However, emerging evidence suggests that tBP coordinates to the Cu(II) species and limits the performance of these electrolytes. To date, the implications of this coordination are poorly understood. Here, the importance of Lewis base additives for the successful implementation of copper complexes as redox mediators in DSCs is demonstrated. Two redox couples, $[Cu(dmp)_2]^{+/2+}$ and $[Cu(dpp)_2]^{+/2+}$ (with dmp = 2,9-dimethyl-1,10-phenanthroline and dpp = 2,9-diphenyl-1,10-phenanthroline) in combination with three different Lewis bases, TFMP (4-(trifluoromethyl)pyridine), tBP, and NMBI (1-methyl-benzimidazole), are considered. Through single-crystal X-ray diffraction analysis, absorption, and ^{1}H-NMR spectroscopies, the coordination of Lewis bases to the Cu(II) centers are studied. This coordination efficiently suppresses recombination losses and is crucial for high performing solar cells. If, however, the coordination involves a ligand exchange, as is the case for $[Cu(dpp)_2]^{+/2+}$, the redox mediator regeneration at the counter electrode is significantly retarded and the solar cells show current limitations.

1. Introduction

The energy transition from fossil fuels to renewable sources requires a mix of different alternative technologies, with energy production from solar energy expected to comprise a substantial share.[1] The price of energy derived from silicon-based solar cells has dropped to be highly competitive with fossil fuel-derived energy over the last decade, rendering them an excellent candidate for large-scale power plants and for rooftop applications. In recent years, DSCs have been established as a highly promising alternative for diffuse and low light conditions.[2–4] DSCs are currently the most efficient solar cell technology in low light conditions, which makes them excellent candidates for building and automobile integrated photovoltaics and to power sensors, appliances for the Internet of Things (IoT), and portable devices.[5–10] Recent developments of new photoanodes, counter electrodes, dyes, and co-adsorption strategies have further improved device efficiencies.[11–28] Furthermore, the

---

Dr. S. O. Fürer, Dr. R. A. Milhuisen, Dr. M. K. Kashif,
Dr. S. R. Raga, Prof. U. Bach
Department of Chemical Engineering
Monash University
Clayton, VIC 3800, Australia
E-mail: udo.bach@monash.edu

Dr. S. O. Fürer, Dr. R. A. Milhuisen, Dr. M. K. Kashif, Dr. S. R. Raga,
Dr. L. Frazer, Dr. A. M. Funston, Prof. U. Bach
ARC Centre of Excellence in Exciton Science
Monash University
Clayton, VIC 3800, Australia

Dr. M. K. Kashif, Dr. N. W. Duffy
CSIRO Energy
Clayton, VIC 3168, Australia

The ORCID identification number(s) for the author(s) of this article can be found under https://doi.org/10.1002/aenm.202002067.

DOI: 10.1002/aenm.202002067

Dr. S. S. Acharya, Dr. C. Forsyth, Dr. L. Frazer, Dr. A. M. Funston
School of Chemistry
Monash University
Clayton, VIC 3800, Australia

Dr. M. Liu, Prof. Y. Tachibana
School of Engineering
RMIT University
Bundoora, VIC 3083, Australia

Prof. C. A. Ohlin
Department of Chemistry
Umeå University
90751, Umeå, Sweden

Prof. U. Bach
Melbourne Centre for Nanofabrication
Australian National Fabrication Facility
Clayton, VIC 3168, Australia

improved stabilities and efficiencies of aqueous DSCs open up new opportunities for the sustainability of these devices.[29–31] Recent trends to replace ruthenium dyes with organic or copper dyes and I^-/I_3^--based electrolytes with earth-abundant transition metals such as cobalt-, iron-, or copper-based electrolytes have opened up new pathways to commercialization.[32–52]

Initially, the motivation to incorporate copper complexes as redox couples in DSCs was based on the crucial role that blue copper proteins play in nature as efficient electron transfer mediators in the photosynthetic chain: the protein environment restricts the geometrical change from the preferred tetrahedral coordination geometry of Cu(I) to square-planar Cu(II), facilitating the electron transfer through reduction of the energy barrier involved in this oxidation.[53] Mimicking this mechanism, Hattori et al. managed to reach efficiencies up to 1.4% at 100 mW cm^{-2} solar irradiation in DSCs with their best performing redox couple $[Cu(dmp)_2][CF_3SO_3]_{1/2}$.[51] Later, Bai et al. significantly enhanced the efficiency to 7.0% using an organic sensitizer and, more recently, efficiencies up to 10.6% have been achieved by changing the counter ion to TFSI$^-$ (bis(trifluoromethane)sulfonimide) and using a PEDOT (poly(3,4-ethylenedioxythiophene)) counter electrode.[49,54] Replacing the phenanthroline ligand with its bipyridine analogue, 4,4′,6,6′-tetramethyl-2,2′-bipyridine, Saygili et al. achieved efficiencies over 10%,[49] which was recently further improved to 11.6% at 1 sun and over 28% under a 1000 lux fluorescent light tube through further optimization of the dye energy levels.[2,55] All electrolyte mixtures employed in these studies have in common that they use tBP and Li$^+$-salts as additives, which have historically been applied in I^-/I_3^--based electrolytes. tBP has been shown to shift the conduction band (CB) edge of TiO_2 toward more negative potentials owing to its Lewis base character and the steric hindrance of the *tert*-butyl group has been reported to significantly reduce recombination through shielding of the titania surface.[56]

In the case of copper electrolytes, this Lewis base character may have a further influence since it is well known that Cu(II) complexes tend to be penta- or hexacoordinated, with the fifth and sixth coordination sites typically occupied by the solvent or the counter ion such as CH_3COO^-, ClO_4^-, or BF_4^-, respectively.[57] Ashbrook and Elliott found tBP kinetically traps Cu(II) complexes, temporarily preventing reduction to Cu(I) when using copper dyes in DSCs.[58] A similar observation was made by Saygili et al. and Kavan et al., who observed a more complex electrochemistry of the bipyridyl based redox couples $[Cu(dmby)_2]^{+/2+}$ and $[Cu(tmby)_2]^{+/2+}$ (with dmbpy = 6,6′-dimethyl-2,2′-bipyridine and tmby = 6,6′,4,4′-tetramethyl-2,2′-bipyridine), respectively, and a shift of the redox potential of $[Cu(dmp)_2]^{+/2+}$ upon addition of tBP.[47,59]

Chemical modification of the ligand to increase the steric hindrance around the metal center can force Cu(II)-complexes into a four-coordinate structure, shielding it from solvent or Lewis base coordination. It was, for instance, shown that the absorption spectra of $[Cu(dpp)_2]^{2+}$ is independent of the solvent in which it was measured, indicating a lack of solvent coordination.[57]

For the cases of dmbpy and 1,8-bis(2′-pyridyl)-3,6-dithiaoctane (PDTO), it was shown that the presence of 10–15 molar equivalents (eq.) of tBP with respect to Cu(II) in the electrolyte leads to a complete ligand exchange of the Cu(II) species.[60,61] The formation of these multispecies redox shuttles was found to be beneficial for their performance in electrolytes for DSCs. For the phenanthroline analogues, however, to-date, the chemical interaction with Lewis bases is still poorly understood. Using density functional theory (DFT) calculations, Saygili et al. predicted a coordination of tBP to the $[Cu(dmp)_2]^{2+}$ complex and have suggested that this coordination induces the shift in rest potential with respect to the tBP-free solution.[62] The induced shift in redox potential caused by coordination with electrolyte additives has been speculated to be a crucial factor for the success of these redox mediators, by significantly reducing the driving force for recombination and therefore allowing for the high open-circuit voltage (V_{OC}) values reported. Very recently, Kannankutty et al. studied the coordination of tBP to $[Cu(dmp)_2]^{2+}$ using absorption and ^{1}H-NMR spectroscopy and concluded that $[Cu(dmp)_2(TBP)(MeCN)_x]^{2+}$ (with $x = 0$, 1) is the most likely species in the electrolyte mixture.[63]

In this work, we present experimental evidence for the coordination of tBP to the Cu(II) metal center and compare it to two other Lewis bases of different binding strength, TFMP and NMBI. Through a comparison with the more shielded $[Cu(dpp)_2]^{2+}$ as a model compound, we present a direct correlation of the coordination of the Lewis bases with the copper species on the device performance. We show that Lewis bases as electrolyte additives are crucial for this class of mediators since they coordinate to the Cu(II) centers which effectively blocks recombination in devices. We present how the selection of additives needs to be carefully adjusted to the steric constraints of the Cu(II) coordination sphere in order to achieve high conversion efficiencies in solar cells. Furthermore, we introduce NMBI as a superior electrolyte additive for Cu-based electrolyte systems that outperforms the state-of-the-art additive tBP in power conversion efficiencies.

2. Results and Discussion

2.1. The Coordination of Lewis Bases with Cu(II)Phenanthroline Complexes

While Cu(I) d^{10} complexes are typically four-coordinate with a tetrahedral geometry, d^9 Cu(II) complexes are usually 5–6 coordinate showing a flattened Jahn–Teller distorted geometry where the axial ligands are elongated with respect to the equatorial Cu-ligand bonds.[57,64] Coordination of Lewis bases to Cu(II) bisphenanthroline complexes is a well-known phenomenon and has been reported to happen on the ps time scale for exciplex formation with excited state $[Cu(II)(dmp)^{\bullet -}(dmp)]^*$ complexes.[65]

Figure 1a shows the absorption spectra of $[Cu(dmp)_2]^{2+}$ in the non-coordinating solvent dichloromethane (CH_2Cl_2), titrated with aliquots of tBP. The absorption band at 524 nm is assigned to a ligand-to-metal charge transfer and the band around 740 nm to a d–d transition.[57] In coordinating solvents, these bands typically vary significantly for copper(II) bisdiimine complexes owing to the formation of a pentacoordinate complex with the solvent (see Figure S1, Supporting Information, for the absorption spectra in CH_3CN). Accordingly, upon addition of

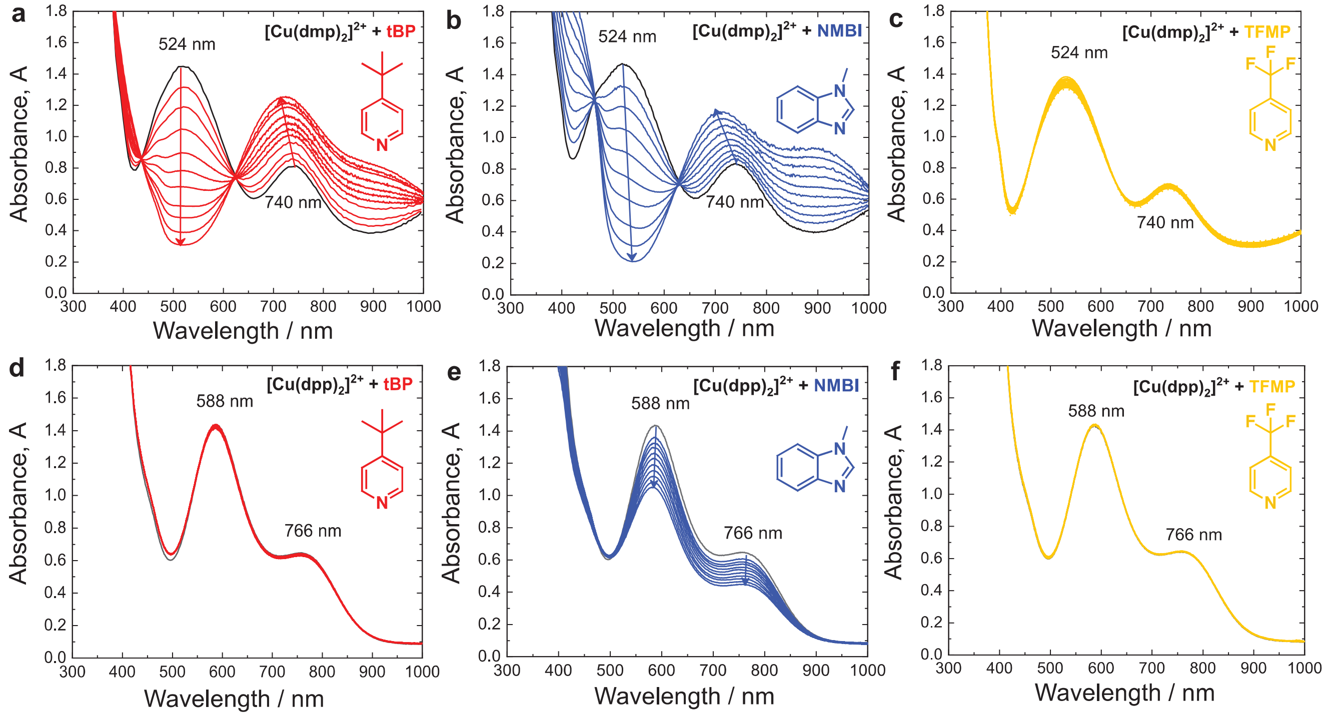

Figure 1. UV–vis absorption spectra of a–c) $[Cu(dmp)_2]^{2+}$ and d–f) $[Cu(dpp)_2]^{2+}$(5 mM) upon the addition of tBP (red), NMBI (blue), TFMP (yellow), and before addition (black) in CH_2Cl_2. Lewis bases were pre-dissolved in CH_2Cl_2 and added in ≈1 µL aliquots (0.1 molar eq.) to the Cu^{2+} complex solutions. Spectra have been corrected for aliquot dilutions.

tBP in 0.1 molar eq. increments to a solution of $[Cu(dmp)_2]^{2+}$, the band at 524 nm continuously decreases, while the shoulder at 740 nm increases and is slightly blue-shifted. With the addition of one full equivalent of tBP there is no further noticeable change in the spectra, indicating a complete reaction at a 1:1 molar ratio (see Figure S2, Supporting Information, for titrations above 1 molar eq.). The appearance of an isosbestic point at 620 nm indicates the absence of any intermediates or side products being formed in this transition.

A similar effect to tBP was observed when titrating $[Cu(dmp)_2]^{2+}$ with NMBI (Figure 1b), another Lewis base that has previously been reported to have similar effects to tBP as an electrolyte additive for DSCs.[39,66–68] In contrast, titration of $[Cu(dmp)_2]^{2+}$ with TFMP causes only minor spectral changes (Figure 1c). While TFMP has similar steric constraints as tBP, it is a significantly weaker Lewis base due to the electron withdrawing nature of the fluoro-substituents and therefore appears to only weakly coordinate to the Cu(II) center. Hence, the coordination appears to correlate with the Lewis basicity of the Lewis bases that increases in the order TFMP < tBP < NMBI.

To investigate the effect of steric constraints on the coordination of Cu-phenanthroline complexes with Lewis bases, we extended our studies to $[Cu(dpp)_2]^{2+}$, in which the Cu(II) metal center is shielded significantly more strongly through the phenyl substituents in the 2- and 9-position of the 1,10-phenanthroline ligand (for the chemical structures see Figure S3, Supporting Information). The steric hindrance around the Cu-center has previously been reported to effectively shield $[Cu(dpp)_2]^{2+}$ from solvent coordination causing the absorption spectra to be solvent independent.[57] Figure 1d–f shows the titration of $[Cu(dpp)_2]^{2+}$ with the three different Lewis bases. Only a slight decrease in absorption was observed upon titration with 1 molar eq. of tBP and only upon addition of several equivalents the two maxima decrease significantly (see Figure S2d, Supporting Information). As in the case of $[Cu(dmp)_2]^{2+}$, no changes were observed in the presence of TFMP. However, upon titration with the strongest of the investigated Lewis bases, NMBI, the peaks at 588 and 766 nm continuously decrease in intensity with no observable shift of the peaks. This observation suggests a different mechanism to the case of $[Cu(dmp)_2]^{2+}$, and indicates the decomposition of $[Cu(dpp)_2]^{2+}$ or at least the formation of a new species with no absorption in the investigated absorption range, such as would be the case for a ligand exchange. As expected, as Cu(I) prefers a four coordinate coordination sphere, Cu(I) complexes of both dmp and dpp experience no change in the absorption spectra with the addition of any of the three Lewis bases (see Figure S4, Supporting Information).

To gain a deeper understanding of the chemical nature of the Lewis base coordination with the Cu(II) complexes, we measured X-ray diffraction of single crystals grown in the presence of tBP or NMBI. Crystals were obtained by slow ether diffusion into solutions of the Cu(II) complexes and 15 molar eq. (the same molar equivalents as in the electrolyte solution for the DSCs, see below) of the Lewis bases in CH_2Cl_2. The crystal structures are shown in **Figure 2** and selected bond lengths are summarized in Table S1, Supporting Information. In agreement with our observations in the titration experiment, we find tBP to take up the fifth coordination site around the copper center of $[Cu(dmp)_2]^{2+}$, forming a distorted trigonal bipyramidal geometry.

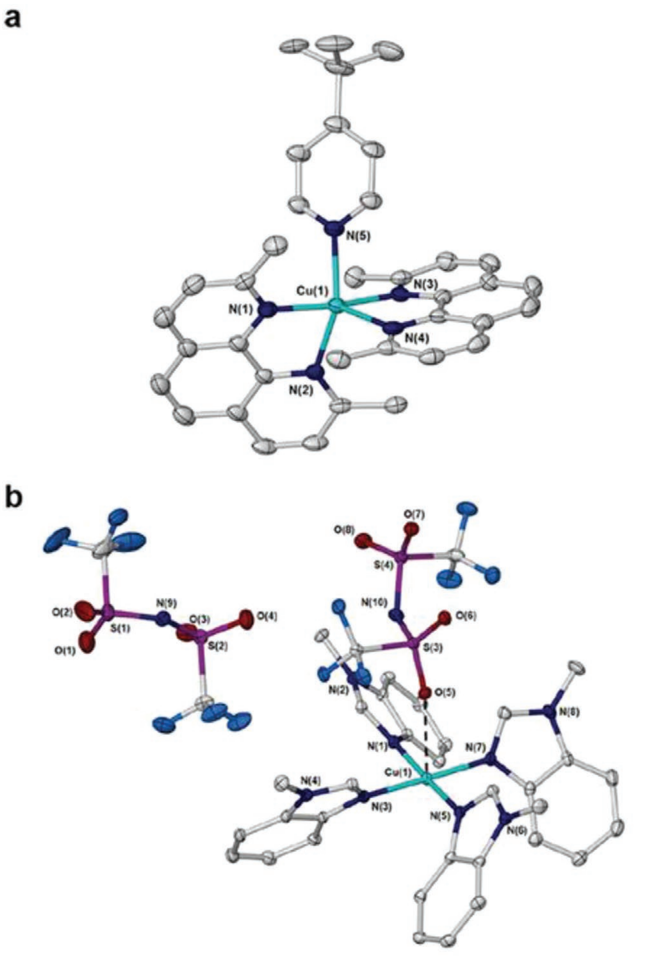

Figure 2. Single crystal X-ray structures of a) $[Cu(dmp)_2(tBP)](TFSI)_2$ and b) $[Cu(NMBI)_4](TFSI)_2$ with non-hydrogen atoms represented by 50% displacement ellipsoids. Hydrogen atoms and the counter TFSI anions in (a) have been omitted for clarity.

$[Cu(dmp)_2(tBP)](TFSI)_2$ crystallizes in a triclinic lattice with a P-1 space group, a structure that is comparable to the previously reported structures of $[Cu(dmp)_2Cl](PF_6)_2$ and $[Cu(dmp)_2(H_2O)](CF_3SO_3)_2$.[69,70]

Our data experimentally confirms the theoretical prediction of a pentacoordinated complex by Saygili et al. based on DFT calculations.[62] This coordination has major implications for the redox chemistry and hence the performance of $[Cu(dmp)_2]^{+/2+}$ as a redox couple in DSCs which will be discussed in further detail later.

Complete ligand exchange was found for crystals grown from $[Cu(dpp)_2]^{2+}$ in the presence of NMBI (Figure 2b) forming the pentacoordinated complex $[Cu(NMBI)_4(TFSI)]^{2+}$. The Cu(II) center is surrounded by four NMBI ligands, the nitrogens arranged in one plane and the fifth coordination site occupied by a weak coordination with one of the oxygens of the $TFSI^-$ counterion showing a pseudo Jahn–Teller distortion. The Cu-N bond lengths of 1.984–1.996 Å indicate a strong coordination with the Lewis base, while the $TFSI^-$ forms a weak Cu-O bond with a bond length of 2.728 Å. The formation of $[Cu(NMBI)_4(TFSI)]^{2+}$ is consistent with the postulated ligand exchange based on our titration experiments where we found a decrease in both absorption maxima with increasing amounts of NMBI present (see Figure 1e). A similar ligand exchange, but with tBP, has previously been reported for 2,2′-bipyridine-based Cu(II) complexes: complete ligand replacement with excess tBP forming $[Cu(tBP)_4]^{2+}$ has been observed by Wang and Hamman for dmbpy and by Hoffeditz et al. for their PDTO ligand.[60,61]

Unfortunately, we were not able to grow crystals suitable for single crystal X-ray diffraction for $[Cu(dmp)_2]^{2+}$ in the presence of NMBI and for $[Cu(dpp)_2]^{2+}$ in the presence of tBP. Therefore, we studied the Lewis base coordination with the two Cu(II) complexes using ^{1}H-NMR. The paramagnetic nature of Cu(II) leads to a broad spectra with no observable peaks in the aromatic region. This allows us to observe the appearance of any aromatic compounds that are not coordinated to the Cu(II) center directly, such as the appearance of a free ligand through ligand exchange with the Lewis bases. Indeed, in the case of $[Cu(dpp)_2]^{2+}$, we were able to detect the appearance of free ligand upon addition of tBP or NMBI, while with the addition of TFMP only the appearance of the free Lewis base was observed (Figures S5–S7, Supporting Information). Through addition of 1 molar eq. of CH_2Cl_2 to the NMR sample as an internal reference, we were able to quantify the amount of free ligand appearing. With the addition of either tBP or NMBI, we detected the appearance of two ligands per copper complex, which suggests a complete ligand exchange for both Lewis bases in combination with $[Cu(dpp)_2]^{2+}$. In contrast, there is no evidence of free ligands in the NMR spectra of $[Cu(dmp)_2]^{2+}$ with the addition of tBP or NMBI (Figures S8–S10, Supporting Information). This suggests that the dmp ligand does not dissociate in the presence of the Lewis bases and supports the postulated formation of a pentacoordinated complex. Apart from the singlet peaks assigned to the methyl groups of tBP (1.3 ppm) and NMBI (4.8 ppm), no distinct signals were observed for the two Lewis bases. The absence of any aromatic signals for the two Lewis bases can be attributed to the fast ligand exchange on an NMR scale with the paramagnetic copper center as previously reported for similar compounds.[60] The appearance of broad peaks in the aromatic region upon addition of TFMP to $[Cu(dmp)_2]^{2+}$ indicates a weak coordination of the TFMP with the paramagnetic Cu(II) center. This suggests the exchange of TFMP is slower on the NMR timescale compared to that of tBP and NMBI, and can therefore be partially resolved.

These solution experiments are in good agreement with our crystal structures and suggest a similar coordination of the Lewis bases with the Cu(II) complexes in solution as in the solid. Combining the crystal structures, ^{1}H-NMR and UV–Vis absorption data, we propose a mechanism of Lewis base coordination to the Cu(II) bisphenanthroline complexes depending on the steric constraints the phenanthroline ligand induces around the Cu(II) center (**Figure 3**). For weakly shielding ligands that sterically allow for pentacoordinated complexes, such as dmp, the Lewis base occupies the fifth coordination site, while for strongly shielding ligands, such as dpp, a ligand exchange occurs in order to form the energetically more favorable pentacoordinated complex.

To investigate the influence of the outlined Lewis base coordination with $[Cu(dmp)_2]^{2+}$ and $[Cu(dpp)_2]^{2+}$ on their redox properties, cyclic voltammograms (CV) of the Cu-complexes

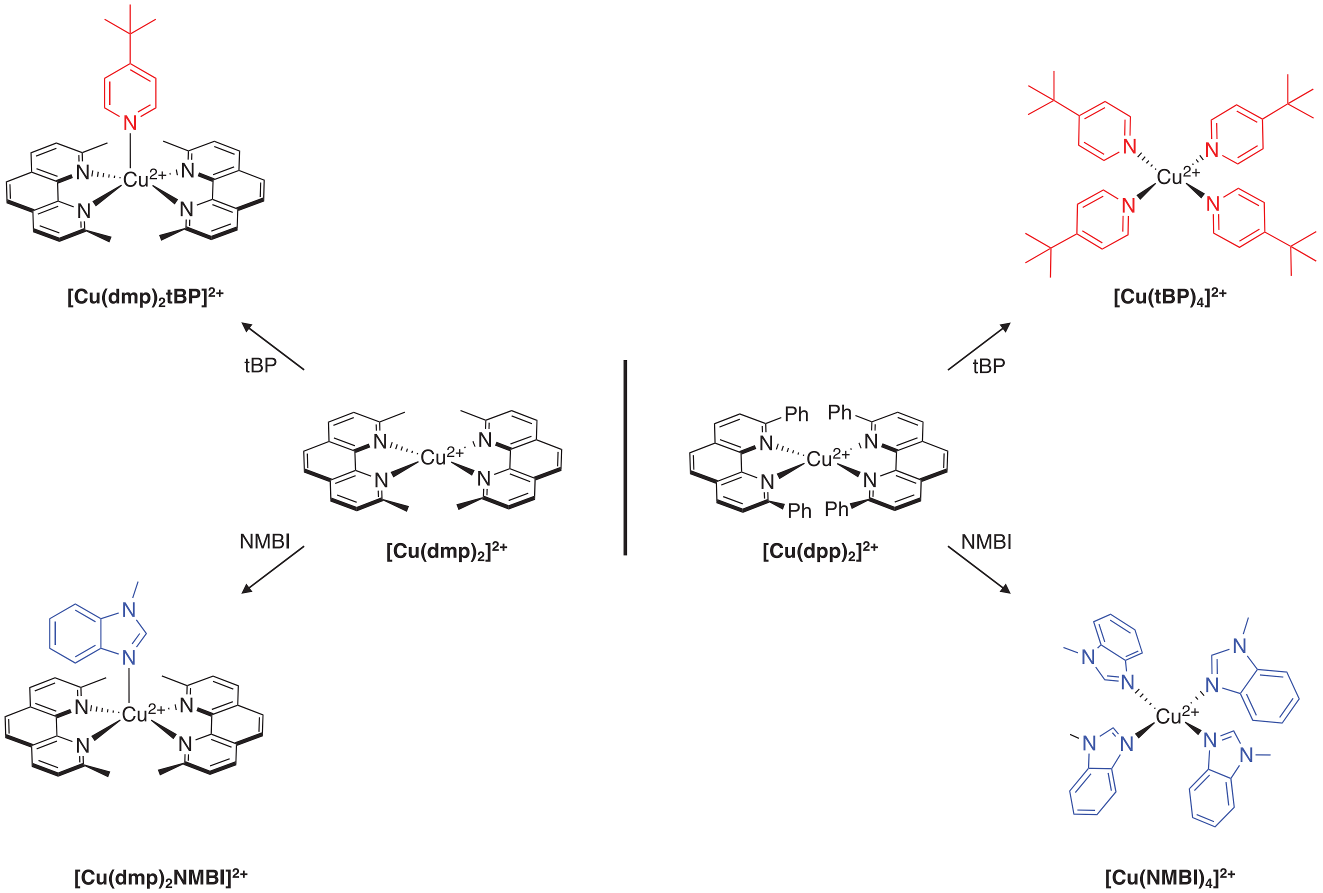

Figure 3. Postulated Lewis-base coordination for the Cu(II)-complexes $[Cu(dmp)_2]^{2+}$ and $[Cu(dpp)_2]^{2+}$. The structures of $[Cu(dmp)_2tBP]^{2+}$ and $[Cu(NMBI)_4]^{2+}$ are based on single crystal analysis shown in Figure 2. The structures of $[Cu(dmp)_2NMBI]^{2+}$ and $[Cu(tBP)_4]^{2+}$ are postulated structures based on our observations from absorption spectra, titration experiments, and ^{1}H-NMR spectroscopy measurements. While the dmp ligand allows for additional coordination of a Lewis base leading to pentacoordinated complexes, the presence of Lewis bases lead to a ligand exchange for the dpp ligand. For simplicity, additional coordination with solvent molecules or counter ions are not shown.

were recorded in the presence and absence of these Lewis bases and are presented in **Figure 4** (see Table S2, Supporting Information, for the electrochemical data). In agreement with previous reports,[47] we found the reduction peak of $[Cu(dmp)_2]^{2+}$ to be strongly affected by the presence of tBP. Upon addition of an increasing amount of tBP, the reduction peak is shifted to lower potentials by up to ≈188 mV for 15 molar eq. (see Figure S11 and Table S2, Supporting Information). As expected, the oxidation peak is only weakly affected by the presence of tBP, and the peak separation therefore increases from 96 mV to ≈252 mV for 15 molar eq. of tBP.

This is in good agreement with our prior observations, that while tBP does not coordinate to $[Cu(dmp)_2]^+$ (Figure S4, Supporting Information), it coordinates to $[Cu(dmp)_2]^{2+}$ to form the pentacoordinated complex $[Cu(dmp)_2tBP]^{2+}$. The coordination of the additional ligand stabilizes the Cu(II) redox state and hence the redox potential is shifted significantly to lower potentials.

Electrochemical systems that are coupled with structural or chemical changes are typically described in a square scheme as shown in **Figure 5**.[72–74] From our absorption, NMR studies, and crystallographic data, we know that **A** and **D** are the two stable forms of the two redox states. Therefore, the electrochemistry is coupled with a Lewis base coordination/dissociation and the redox couple is better presented as $[Cu(dmp)_2]^+$/$[Cu(dmp)_2LB]^{2+}$ (with LB = NMBI or tBP). In principle, the oxidation from **A** and **D** can follow one of three different pathways: oxidation followed by coordination (**ACD**), coordination followed by oxidation (**ABD**), or a concerted pathway (**AD**). From the absorption spectra of $[Cu(dmp)_2]^+$ in the presence of tBP (Figure S4, Supporting Information), we know that tBP is not interacting with $[Cu(dmp)_2]^+$. Therefore, we can assume that the equilibrium between **A** and **B** is shifted more strongly to the left, which makes pathway **ACD** the most likely. This is supported by the small change of the oxidation peak in the presence of tBP.

For the reduction starting from $[Cu(dmp)_2LB]^{2+}$, again, the same three pathways are conceivable: Lewis base dissociation followed by reduction (**DCA**), reduction followed by LB dissociation (**DBA**) or a concerted reaction (**DA**). Based on the quantitative formation of $[Cu(dmp)_2LB]^{2+}$ upon titration of tBP or NMBI to $[Cu(dmp)_2]^{2+}$ (Figure 1) and the 15 molar eq. of LB present in the CV, we can assume that the equilibrium between **C** and **D** is pushed far to the right. Accordingly, we observe a strong shift of the reduction peak towards lower potentials and the **DBA** pathway seems the most likely.

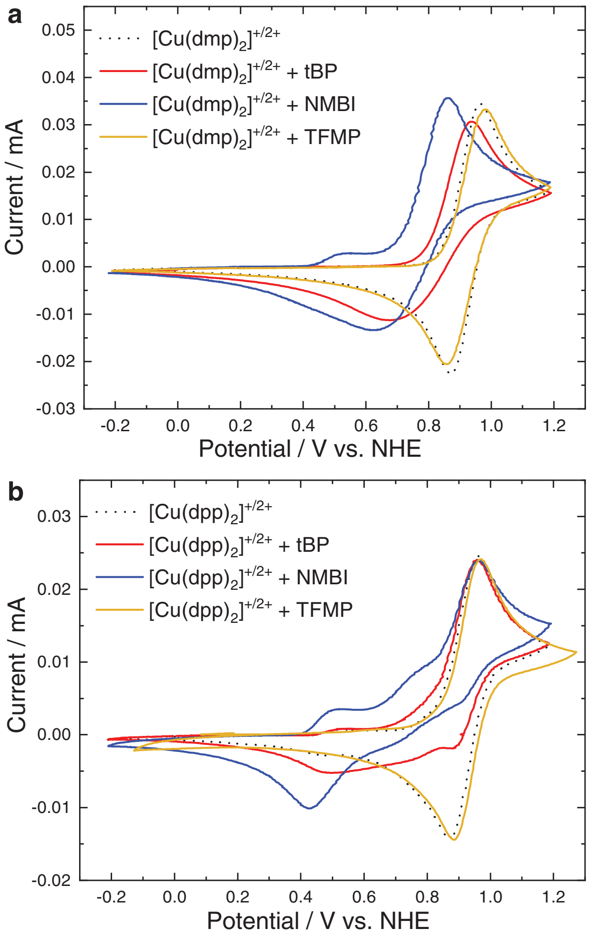

Figure 4. Cyclic voltammograms of a) [Cu(dmp)$_2$]$^+$ and b) [Cu(dpp)$_2$]$^+$ in the absence (black dotted) and presence of 15 molar eq. of tBP (red), NMBI (blue), and TFMP (yellow). CVs were performed inside a N$_2$ glovebox on 4.6 mM solutions of each Cu(I) complex in CH$_3$CN in the presence of 0.1 M TBAPF$_6$ as a supporting electrolyte, and measured at a scan rate of 100 mV s^{-1}. CVs are plotted in V versus NHE after conversion with $E_{1/2}$(Fc) = 0.63 V versus NHE.[71]

In the presence of NMBI, the oxidation peak of [Cu(dmp)$_2$]$^{+/2+}$ is shifted by 96 mV to lower potential. An additional peak arises at 0.5 V, which can be assigned to the oxidation of NMBI itself (Figure S12, Supporting Information). Therefore, NMBI can be oxidized by the Cu(II) species, which explains the appearance of [Cu(dmp)$_2$]$^+$ in the ^{1}H-NMR of [Cu(dmp)$_2$]$^{2+}$ in the presence of 15 molar eq. NMBI (Figure S9b, Supporting Information). No change in redox behavior was observed in the presence of TFMP, which is in accordance with our observations in the absorption spectra and confirms again that TFMP either does not or only weakly interacts with the copper complexes.

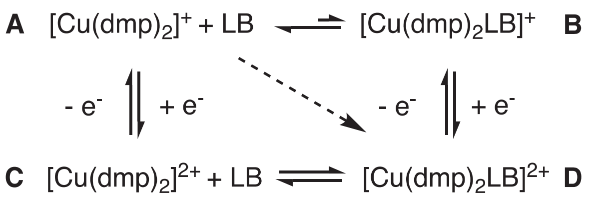

Figure 5. Square scheme for the reduction of [Cu(dmp)$_2$LB]$^{2+}$ with LB = NMBI or tBP. Species **A** and **D** are the reduced and oxidized form of the redox couple that were experimentally determined. The oxidation is postulated to follow the pathway **ACD**, while the reduction is understood to follow **DBA** since the equilibrium between **C** and **D** is pushed to the right owing to the excess of tBP present in the solution.

For [Cu(dpp)$_2$]$^{+/2+}$ (Figure 4b), the reduction is coupled with ligand exchange of the dpp ligand with the Lewis bases leading effectively to a [Cu(dpp)$_2$]$^+$/[Cu(LB)$_4$]$^{2+}$ redox couple. This allows for several intermediate structures to be formed and is manifested in the complex reduction behavior in the CV. Similar observations have been reported for the cyclic voltammograms of [Cu(PDTO)]$^+$/[Cu(tBP)$_{4+x}$]$^{2+}$ and of [Cu(dmbpy)$_2$]$^+$/[Cu(tBP)$_y$]$^{2+}$, which also involve complete ligand exchange with tBP involving several intermediate complexes.[60,61]

2.2. Solar Cell Performance

The observed coordination of the Lewis bases to the copper complexes has significant implications on the performance of these compounds as redox mediators in dye-sensitized solar cells. DSCs incorporating Cu$^{+/2+}$ based electrolytes sandwiched between Y123-sensitized TiO$_2$ photoelectrodes and PEDOT counter electrodes were fabricated and measured under simulated sunlight. **Figure 6** shows *J*–*V* curves in the dark and under illumination of the champion devices incorporating [Cu(dmp)$_2$]$^{+/2+}$ or [Cu(dpp)$_2$]$^{+/2+}$ as redox couples. The photovoltaic parameters averaged over three devices for each electrolyte composition are summarized in Table S3, Supporting Information, and the parameters of the champion devices are shown in Table S4, Supporting Information. The electrolyte solutions comprised 0.2 M Cu(I) complex, 0.04 M Cu(II) complex, 0.1 M LiTFSI, and 0.6 M Lewis base in CH$_3$CN. In the absence of any Lewis base, both redox couples show a low solar cell performance with efficiencies of 1.21% and 0.05% for [Cu(dmp)$_2$]$^{+/2+}$ and [Cu(dpp)$_2$]$^{+/2+}$, respectively. The devices suffer from low V_{OC}, J_{SC}, and FF. In particular, the [Cu(dpp)$_2$]$^{+/2+}$ redox couple shows high dark currents leading to a V_{OC} of only 160 mV for the best performing device. Upon addition of tBP or NMBI in the electrolyte, the performance of DSCs in combination with either of the copper complexes is significantly improved, and V_{OC} values of over 1.0 V were achieved. In contrast, V_{OC} values of 700–750 mV were obtained in the presence of TFMP.

The addition of NMBI to the [Cu(dmp)$_2$]$^{+/2+}$ electrolyte increases the J_{SC} more than threefold to 12.4 mA cm^{-2} with respect to the Lewis base-free control device, while the V_{OC} is boosted by over 400 mV to 1.05 V, leading to a champion efficiency of 9.19%. A similar V_{OC} was achieved for tBP-containing devices with a J_{SC} of 10.8 mA cm^{-2}, leading to an efficiency of 7.84%. Devices based on [Cu(dpp)$_2$]$^{+/2+}$ generally show lower efficiencies compared to their dmp analogues, which is mainly attributed to the complex redox behavior and charge-transfer limitations at the counter electrode, which will be discussed in further detail later. However, for both redox couples, the presence of NMBI and tBP significantly improves the efficiencies, while TFMP improves the performance of devices incorporating [Cu(dpp)$_2$]$^{+/2+}$, but is detrimental to devices with [Cu(dmp)$_2$]$^{+/2+}$.

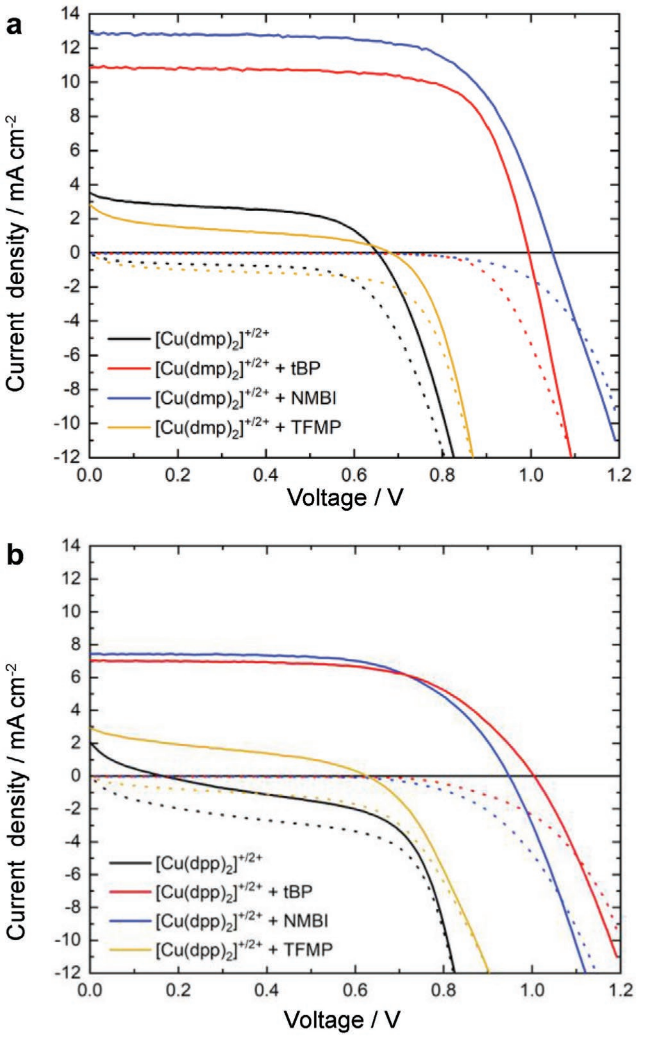

Figure 6. *J–V* curves for champion DSCs employing a) $[Cu(dmp)_2]^{+/2+}$ and b) $[Cu(dpp)_2]^{+/2+}$-based electrolytes in conjunction with Y123-sensitized TiO_2 photoanodes and PEDOT counter electrodes, measured under dark conditions (dotted lines) and simulated standard AM 1.5G irradiation at 100 mW cm^{-2} (solid lines). All electrolytes comprised of 0.2 м Cu(I) complex, 0.04 м Cu(II) complex, and 0.1 м LiTFSI in CH_3CN with no additive (black), or 0.6 м of additive, tBP (red), NMBI (blue), or TFMP (yellow).

Electrolyte additives such as Li^+ and tBP are typically added to fine tune the energy levels in DSCs and boost the efficiency of the devices. Li^+ is known to be a flatband potential determining ion in aprotic solvents through adsorption on and intercalation into the polycrystalline TiO_2 surface.[75] This lowers the CB of TiO_2 and facilitates an efficient injection of electrons into the TiO_2. Lewis bases such as tBP displace some of those cations and shift the conduction band edge and trap levels in TiO_2 toward higher energies.[56,76] This allows for higher open-circuit potentials since the V_{OC} is determined by the difference of the quasi Fermi level of electrons in the TiO_2 and the redox potential of the electrolyte. Furthermore, tBP plays an important role in blocking recombination from electrons in the TiO_2 film with the oxidized species of the electrolyte.[77] By fine tuning the ratio of Li^+ and tBP, the solar cell performance can be maximized.

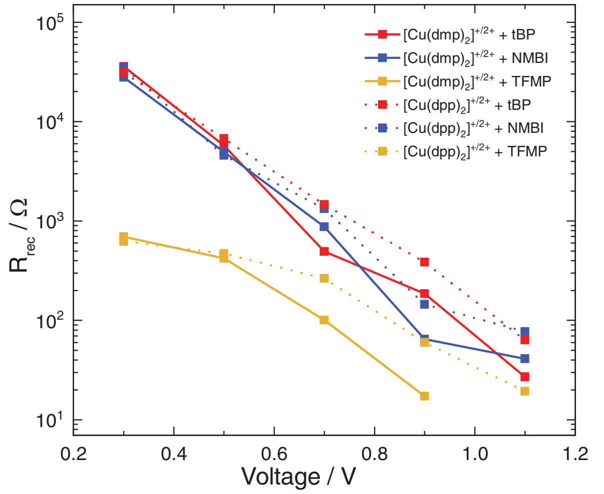

Figure 7. Recombination resistance (R_{rec}) extracted from impedance spectroscopy data for DSCs employing $[Cu(dmp)_2]^{+/2+}$ (solid lines) and $[Cu(dpp)_2]^{+/2+}$ (dotted lines) electrolytes in the presence of tBP (red), NMBI (blue), and TFMP (yellow), measured at various applied voltages under constant white light LED irradiation.

NMBI and TFMP have previously been reported to shift conduction band edge of TiO_2 to a similar extent to tBP, and all three Lewis bases have shown efficient blocking of recombination with $Co^{2+/3+}$ and I^-/I_3^- electrolytes.[66,67,78–80] However, in our devices, TFMP shows no or significantly less improvement in the V_{OC} with respect to tBP and NMBI. This indicates that the described adsorption on the TiO_2 surface alone cannot explain the boost in V_{OC} in our devices. In addition to the surface modification, the Lewis bases have to either increase the redox potential of the electrolyte or increase the quasi-Fermi level of the TiO_2 in order to cause the observed gain in V_{OC}. In our cyclic voltammograms (Figure 4), we found that tBP and NMBI both shift the redox potential of the copper complexes toward lower potentials, which would lead to smaller V_{OC} in DSCs and hence cannot explain our observations. We therefore conclude that the number of electrons in the TiO_2 needs to be significantly increased to explain the higher V_{OC}; in other words, the recombination between electrons in the titania with the Cu(II) species in the electrolyte is significantly suppressed. We hypothesize that the described coordination of the Lewis bases with the Cu^{2+} complexes itself plays a crucial part in this process.

To test this hypothesis, we performed impedance spectroscopy on full DSC devices (see Figures S13–15, Supporting Information).[81,82] The spectra were fitted to the equivalent circuit shown in Figure S14, Supporting Information, and the extracted recombination resistance, R_{rec}, is shown in **Figure 7**. For both redox couples, $[Cu(dmp)_2]^{+/2+}$ and $[Cu(dpp)_2]^{+/2+}$, R_{rec} is an order of magnitude larger for devices containing tBP and NMBI with respect to TFMP. For Lewis base-free electrolytes, recombination for these DSCs could not be isolated owing to overlapping semicircles in the Nyquist plots (see Figure S15, Supporting Information). Despite the fact that a value could not be fitted, the merged arcs suggest small values for R_{rec} in comparison with the charge transfer resistance at the counter electrode (R_{CE}), in agreement with the low V_{OC} for these devices. These findings are further supported by recombination lifetimes extracted from intensity modulated photovoltage spectroscopy (IMVS; Table S5 and Figure S16, Supporting Information). The addition of any of the three Lewis bases to the redox couples significantly increases the electron lifetime and hence reduce recombination at the TiO_2/electrolyte interface. However, both tBP and NMBI show a two times longer electron lifetime with respect to TFMP. On the other hand, electron transit times extracted from intensity modulated photocurrent spectroscopy (IMPS) do not depend significantly on the presence or absence of Lewis bases in the electrolyte. This suggests that, while the adsorption of all three Lewis bases to the TiO_2 surface helps to reduce recombination, the coordination of NMBI and tBP with the Cu(II) complexes is the main reason for the efficient blocking of recombination. This is supported by our discussion of the CV in Figure 4, where we found that, upon addition of tBP and NMBI, the reduction peak is shifted significantly. This shift of several hundreds of mV significantly reduces the driving force for recombination of electrons in the TiO_2 with $[Cu(dmp)_2LB]^{2+}$ and $[Cu(LB)_4]^{2+}$, respectively. Accordingly, this is reflected in the high recombination resistance and long electron lifetimes measured with impedance spectroscopy and IMVS, respectively. It is therefore the coordination of NMBI and tBP to the Cu(II) centers and the formation of $[Cu(dmp)_2LB]^{2+}$ and $[Cu(LB)_4]^{2+}$ itself that lowers recombination losses of these electrolytes and allows for the higher solar energy conversions.

J_{SC} is the second parameter that is significantly increased upon addition of Lewis bases to the electrolyte solution. As it is the case for V_{OC}, it is mainly the addition of tBP and NMBI that improves the performance, while the presence of TFMP has a less significant influence. J_{SC} can be expressed as a function of the light-harvesting efficiency (LHE), electron injection, dye regeneration, and charge collection efficiency.[83] Since no coordination of tBP and NMBI with the Cu(I) complexes was observed (Figure S4, Supporting Information) and the shifts in the cyclic voltammograms increase the driving force for dye regeneration, the addition of these Lewis bases should not negatively affect the regeneration process of the oxidized dye.

The LHE could be affected through quenching of the excited dye with the Cu(II) species and, indeed, previous reports have indicated dynamic quenching for $[Cu(dmp)_2]^{2+}$ in combination with LEG4,[48] an organic dye structurally similar to the dye Y123 used in our studies. Dynamic quenching implies exciplex formation. If dynamic quenching was a significant loss mechanism, we would expect the coordination of the Lewis bases to the Cu(II)-centers to significantly reduce the quenching process given that the same oxidized electrolyte species, as discussed above, would be involved. We therefore used time-correlated single photon counting (TCSPC) to test if tBP has an influence on the quenching of the photoluminescence of Y123 by the Cu(II) mediator (see Figure S17, Supporting Information). In contrast to previously reported TCSPC data,[48] we found the fluorescence quenching of Y123 anchored to Al_2O_3 to be mostly not dynamic. These results are consistent with static complexation, rather than exciplex formation. More importantly, we found the decay rate to be largely unaffected by the presence of tBP, which suggests that the LHE is not affected by the presence of Lewis bases in the electrolyte. Similarly, steady-state fluorescence measurements of Y123 on Al_2O_3 in contact with tBP-free and tBP-containing $[Cu(dmp)_2]^{+/2+}$ electrolytes (see Figure S18, Supporting Information) were conducted, which confirm static complexation to be occurring, but more importantly indicate tBP to have little influence on this process. Hence, the increased J_{SC} in the presence of tBP and NMBI is not caused by an improved LHE.

If we make the reasonable assumption that the presence of NMBI and tBP should not influence the electron injection, the improved J_{SC} can be assigned to an improved charge collection efficiency (η_c). In agreement with previous reports,[84] the electron transit times obtained from our IMPS measurements suggest that the electron transport within the TiO_2 semiconductor does not depend on the addition of Lewis bases to the electrolyte solution. Therefore, since only the Lewis base is changed from one device to the other, we can conclude that the electron transport within the TiO_2 semiconductor does not differ between devices and η_c depends on recombination only. The recombination is influenced by the electron occupancy of trap and CB states of the TiO_2 film and the oxidized species in the electrolyte,[79] both of which are influenced by the presence of Lewis bases as discussed above. The high dark currents in the absence of tBP and NMBI (dotted lines in Figure 6) suggest recombination directly from the FTO or the compact TiO_2 to the electrolyte. Hence, the same mechanism of Lewis base coordination with the Cu(II) complexes that reduces the recombination rate at the mesoporous TiO_2 applies at this interface as well. The low photocurrents for the control and the TFMP-containing devices, therefore, arise from a high recombination in these devices.

Interestingly, despite having similar dark current behavior and recombination rates for a given Lewis base additive, $[Cu(dpp)_2]^{+/2+}$ generally shows lower performance than $[Cu(dmp)_2]^{+/2+}$. This mainly arises from both lower photocurrent densities and fill factors. These parameters are largely influenced by the electrolyte through recombination, dye regeneration, competing absorption with the dye, diffusion resistance, and regeneration at the counter electrode. As outlined above, the small differences in the recombination behavior cannot explain the observed difference. Therefore, we further explored the performance differences by analyzing the dye regeneration. The dye regeneration kinetics were determined by transient absorption spectroscopy (Figure S19 and Table S6, Supporting Information) and show an efficient and fast dye regeneration for both electrolytes. In fact, the sterically more constrained $[Cu(dpp)_2]^{+/2+}$ regenerates the oxidized dye even faster than $[Cu(dmp)_2]^{+/2+}$, which we attribute to its higher self-exchange rate owing to a lower reorganization energy of this redox reaction.[51] Our DFT calculations confirm that due to the sterically more restraining phenyl substituents, $[Cu(dpp)_2]^{+/2+}$ shows a lower reorganization energy of 32.4 kJ mol^{-1} with respect to 58.2 kJ mol^{-1} for $[Cu(dmp)_2]^{+/2+}$ (Figure S20 and Table S7, Supporting Information), allowing for a faster regeneration of the dye.

To investigate if competing absorption with the dye is the origin for the difference between the redox couples, incident photon-to-electron conversion efficiency (IPCE) measurements for electrolytes from both Cu-systems in combination with tBP were measured and are presented in Figure S21b, Supporting

Information. For both copper redox couples, the IPCE is improved significantly upon addition of tBP. This indicates the large recombination loss for the copper electrolytes in absence of tBP, even at short-circuit conditions. The comparable integrated current densities of the IPCE going from one copper system to the other in the presence (11.5 vs. 10.4 mA cm^{-2}) or absence (1.88 vs. 1.53 mA cm^{-2}) of tBP, respectively, indicate only minor competing absorption of the electrolyte species with the dye. This is consistent with the low extinction coefficients for both $[Cu(dmp)_2]^+$ and $[Cu(dpp)_2]^+$ (7.8 × 10^3 and 3.1 × 10^3 M^{-1} cm^{-1}), with respect to the dye Y123 (5.3 ×·10^4 M^{-1} cm^{-1} at 532 nm in THF).[85]

Short-circuit currents at different light intensities (Figure S21c, Supporting Information) show a positive linear dependence for $[Cu(dmp)_2]^{+/2+}$, while $[Cu(dpp)_2]^{+/2+}$ shows a sublinear relation, which is typically associated with mass transport limitations of the mediator or charge transfer resistance at the counter electrode.[86] It is worth noting that, at 0.1 sun, the current densities are very similar between the two electrolytes (1.14 and 1.46 mA cm^{-2} for $[Cu(dpp)_2]^{+/2+}$ and $[Cu(dmp)_2]^{+/2+}$, respectively), indicating a comparable electrolyte performance at low light intensities, which is reflected in the similar IPCE spectra. To gain deeper understanding of the diffusion limitations and the electrolyte regeneration at the counter electrode, symmetrical PEDOT-PEDOT devices were prepared. Electrolyte solutions were sandwiched between two PEDOT electrodes and impedance spectra were recorded at 0 V in the dark. The spectra were fitted to an equivalent circuit similar to the one shown in Figure S14, Supporting Information, except for the $R_{\text{rec}}\text{-}CPE_{\mu}$ element. Surprisingly, the diffusion constants, D, obtained from impedance spectroscopy shows a negligible influence on the presence or absence of the Lewis bases (see Table S8, Supporting Information). However, while the resistance at the counter electrode, R_{CE}, for $[Cu(dmp)_2]^{+/2+}$ and $[Cu(dpp)_2]^{+/2+}$ is negligible in the Lewis base free electrolyte solutions and in presence of TFMP, it is significantly increased in the presence of tBP and NMBI. Charge transfer resistances of 5.7 and 7.0 Ω cm^2, respectively, for tBP and NMBI with $[Cu(dmp)_2]^{+/2+}$ were obtained, while 101 and 31.9 Ω cm^2, respectively, were measured for $[Cu(dpp)_2]^{+/2+}$. In other words, the formation of $[Cu(dmp)_2LB]^{2+}$ and $[Cu(LB)_4]^{2+}$, that slows down recombination, also slows down the regeneration at the counter electrode. The high R_{CE} values for electrolytes with tBP and NMBI are in agreement with the complicated redox behavior and strongly shifted reduction peaks observed in the cyclic voltammetry. The high charge transfer resistance of $[Cu(dpp)_2]^{+/2+}$-based devices clearly limits their performance and is the critical difference between the two redox couples.

In summary, we propose a mechanism, as shown in **Figure 8**, using $[Cu(dmp)_2]^{+/2+}$ in combination with tBP as an example. $[Cu(dmp)_2]^+$ efficiently regenerates the oxidized dye molecules (step 1). On oxidation from Cu$^+$ to Cu^{2+}, the copper complex coordination geometry is flattened allowing for coordination of a tBP molecule (step 2). The formation of the pentacoordinated complex stabilizes the Cu(II) redox state, which reduces the driving force for recombination. In the DSC this efficiently reduces recombination with electrons in the TiO$_2$. In step 3, the same mechanism slows down the regeneration of the electrolyte at the counter electrode. Finally, with the release of the coordinating tBP, $[Cu(dmp)_2]^+$ is formed in step 4 in its preferred four-coordinate tetrahedral state.

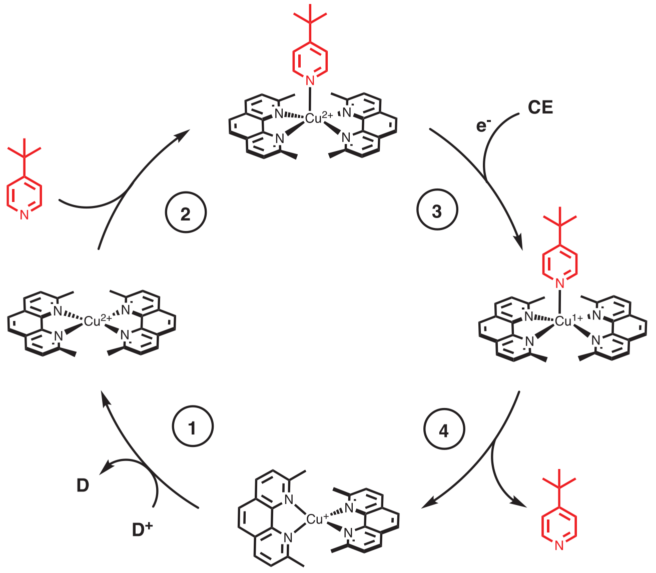

Figure 8. Proposed mechanism for the working principle of Cu$^{+/2+}$ electrolytes in the presence of tBP or NMBI using the example of $[Cu(dmp)_2]^{+/2+}$with tBP. 1) $[Cu(dmp)_2]^+$ effectively reduces the oxidized dye molecule (D$^+$ → D). Upon oxidation, the Cu-complex changes from a tetrahedral to a pseudo square planar coordination sphere. 2) The flattened coordination sphere of the Cu(II) complex allows for the formation of a pentacoordinated complex which efficiently reduces recombination with electrons in the TiO$_2$ film with the Cu(II) complexes. 3) Reduction at the counter electrode. 4) Due to the preferred tetrahedral coordination sphere of Cu(I), tBP is released again.

For $[Cu(dmp)_2]^{+/2+}$, the slow reduction at the counter electrode is not a limiting factor in DSCs and high solar cell efficiencies can be achieved. In the case of $[Cu(dpp)_2]^{+/2+}$, however, the complete ligand exchange with tBP and NMBI limits the electrolyte regeneration at the counter electrode, thereby limiting the current outputs of devices.

3. Conclusion

In conclusion, we were able to demonstrate that the coordination of strong Lewis bases such as tBP and NMBI with Cu(II) phenanthroline complexes is crucial for their performance as electrolytes in DSCs. The coordination of the Lewis bases to the Cu(II) center efficiently slows down recombination. If a weaker Lewis base, such as TFMP is used, no coordination to the Cu(II) center occurs and the DSCs show a significantly reduced performance. For $[Cu(dmp)_2]^{2+}$, we found the oxidized redox species to be the pentacoordinated complex $[Cu(dmp)_2LB]^{2+}$. In the case of $[Cu(dpp)_2]^{2+}$, we observed a ligand exchange with the Lewis bases to form $[Cu(LB)_4]^{2+}$. We generally observed lower performance in DSCs with the latter owing to limitations at the counter electrode. With NMBI, we successfully introduced a new Lewis base as an additive for Cu-phenanthroline based electrolytes that outperforms the commonly used additive tBP.

With this study, we could not only show how the Lewis bases interact with the Cu-mediators, but also how their presence is a necessity for high-performing solar cells. We outlined the importance of fine tuning the Cu(II) complex–Lewis base coordination and the Cu^{2+}-reduction at the counter electrode in order to have an efficient electrolyte regeneration for high efficiencies in devices. While Lewis base coordination is beneficial for $Cu^{+/2+}$ based electrolytes, ligand dissociation complicates the redox behavior and slows down the regeneration kinetics. Further optimization of this coordination, including for the widely used bipyridine analogues, will enable further improvements in this field and allow for open circuit voltages well above 1.1 V.

4. Experimental Section

General Information: Unless specified, all chemicals were purchased from VWR and used without further purification. Anhydrous acetonitrile (CH_3CN), copper iodide, lithium trifluoromethanesulfonate (LiTFSI), and nitrosonium tetrafluoroborate ($NOBF_4$) were purchased from Sigma-Aldrich; petroleum benzine and diethyl ether from Merck. 2,9-diphenyl-1,10-phenanthroline was synthesized according to a previously reported procedure.[87] NMR spectra were recorded on a Bruker Avance III 400 instrument and are referenced versus residual solvent peaks with respect to δ(TMS) = 0 ppm. CHNS analysis was measured by The Campbell Microanalytical Laboratory, University of Otago, New Zealand.

Synthesis: $[Cu(dmp)_2][TFSI]$ and $[Cu(dmp)_2][TFSI]_2$ were synthesized according to a previously published procedure.[49] CuI (229 mg, 1.20 mmol) was added to a solution of neocuproine hemihydrate (580 mg, 2.40 mmol) in 20 mL ethanol and stirred for 3 h. LiTFSI (1.72 g, 6.00 mmol) was added and the mixture stirred overnight. The red precipitate was collected by filtration, washed with water and diethyl ether, and dried in vacuo (815 mg, 1.07 mmol, 89%). ^1H-NMR (400 MHz, $CDCl_3$, δ): 8.48 (d, *J* = 8.3 Hz, 1H), 8.02 (s, 1H), 7.77 (d, *J* = 8.3 Hz, 1H), 2.44 (s, 3H); ESI MS *m*/*z*: 479.1 $[M\text{-}TFSI]^+$, 279.9 $[TFSI]^-$; Anal. calcd for $C_{30}H_{24}CuF_6N_5O_4S_2^-$: C 47.40, H 3.18, N 9.21, S 8.43%; found: C 47.46, H 3.04, N 9.23, S 8.56.

$[Cu(dpp)_2][TFSI]$ was synthesized in analogy using CuI (106 mg, 0.557 mmol), 2,9-diphenyl-1,10-phenanthroline (407 mg, 1.22 mmol), and LiTFSI (800 mg, 2.79 mmol). Petroleum benzine was used to precipitate the product and $[Cu(dpp)_2][TFSI]$ was obtained as an dark red, crystalline solid (499 mg, 0.494 mmol, 81%). ^1H-NMR (400 MHz, $CDCl_3$, δ): 8.50 (d, *J* = 8.3 Hz, 1H), 8.02 (s, 1H), 7.87 (d, *J* = 8.3 Hz, 1H), 7.39 (dd, *J* = 8.3, 1.2 Hz, 2H), 6.84–6.75 (m, 1H), 6.58–6.48 (m, 2H); ESI MS *m*/*z*: 727.1 $[M\text{-}TFSI]^+$, 279.8 $[TFSI]^-$; Anal. calcd for $C_{50}H_{32}CuF_6N_5O_4S_2$: C 59.55, H 3.20, N 6.94, S 6.36%; found: C 59.77, H 3.32, N 6.88, S 6.36. The crystal structure is shown in Figure S22, Supporting Information.

$[Cu(dmp)_2][TFSI]_2$ was prepared by adding $NOBF_4$ (100 mg, 0.856 mmol) to a solution of $[Cu(dmp)_2][TFSI]$ (500 mg, 0.658 mmol) in CH_3CN in an N_2 atmosphere and stirring the mixture for 1h. LiTFSI (900 mg, 3.13 mmol) was added and the mixture was stirred for 5 h. The solvent was removed, and the purple residue redissolved in dichloromethane, filtered through Celite, and added dropwise to diethyl ether. After stirring for 15 min, the precipitate was filtered off, washed with diethyl ether, and dried in vacuo to obtain the product as a purple powder (487 mg, 0.468 mmol, 71%). Anal. calcd for $C_{32}H_{24}CuF_{12}N_6O_8S_4$: C 36.94, H 2.33, N 8.08, S 12.33%; found: C 36.96, H 2.36, N 7.99, S 12.5.

$[Cu(dpp)_2][TFSI]_2$ was synthesized following the same procedure using $[Cu(dpp)_2][TFSI]$ (200 mg, 0.198 mmol), $NOBF_4$ (28.0 mg, 0.240 mmol), and LiTFSI (320 mg, 1.11 mmol). The product was obtained as a black solid (198 mg, 0.154 mmol, 78%). Anal. calcd for $C_{52}H_{32}CuF_{12}N_6O_8S_4$ C 48.47, H 2.50, N 6.52, S 9.95%; found C 48.69, H 2.57, N 6.46, S 9.95.

Absorption Spectroscopy: Absorption spectra were measured on a Perkin Elmer 950 or an Agilent Technologies spectrometer using a 1 cm path length quartz cuvette.

Electrochemical Characterization: Cyclic voltammetric (CV) measurements for electrochemical characterizations were conducted under inert conditions inside a glovebox using a three-electrode configuration employing a 3 mm diameter platinum working electrode, a Ag/AgCl reference electrode, and a platinum wire counter electrode. A Bio-Logic VSP potentiostat was used in CV mode to record current–voltage characteristics of the three-electrode set-up. Measurements were performed at a scan rate of 100 mV s^{-1} (unless otherwise specified) on 4.6 mM solutions of the Cu(I) complex of interest in CH_3CN with 0.1 M $TBAPF_6$ as a supporting electrolyte. Ferrocene was used as for internal calibration and the redox potentials converted with respect to NHE using the standard value $Fc^+/Fc = 0.63$ V versus NHE in CH_3CN.[71]

Device Fabrication and Photovoltaic Performance Data of Devices Employing Copper Complex Electrolytes in the Presence of Lewis Bases: Devices were fabricated with a ≈8 µm mesoporous TiO_2 layer (5 µm of 30 nm TiO_2 particles + 3 µm of 400 nm TiO_2 particles) and were sensitized with the dye Y123. The underlying blocking layer was deposited by dipping the substrates three times into a 10 mM aqueous solution of $TiCl_4$ at 70 °C. The electrolytes comprised 0.20 M Cu(I) complex, 0.04 M Cu(II) complex, 0.10 M LiTFSI, and 0.6 M of Lewis base (NMBI, tBP or TFMP) in CH_3CN as indicated. For the counter electrodes, PEDOT was electrodeposited on ITO-glass as described previously.[86] The electrodes were fused together with a 25 µm hot-melt Surlyn gasket and the electrolyte was filled through one of two pre-drilled holes of the PEDOT electrode inside a N_2 glovebox. Surlyn-coated aluminium foil heated to 120 °C was used to seal the holes. Wires were soldered to each electrical contact for testing. Three devices of each electrolyte composition were fabricated and tested to ensure reproducibility of the data. Current–voltage characteristics were recorded at 100 mW cm^{-2} using a Keithley source meter and an Oriel solar simulator equipped with a xenon lamp and an AM 1.5G filter.

Electrochemical Impedance Spectroscopy: Electrochemical impedance spectroscopy (EIS) was performed using a Zahner Zennium Electrochemical Work Station ECW IM6 as a frequency response analyzer, with a voltage sinusoidal perturbation of 10 mV at a frequency range from 1 Hz to 1 MHz. The DSCs were measured under illumination of a white LED adjusted to provide the same J_{SC} on the devices than 100 mW cm^{-2} AM 1.5 conditions; the DC voltage was varied from 0.3 to 1.2 V. The impedance spectra (Nyquist plots) were fitted to the equivalent circuit shown in Figure S14, Supporting Information, using ZView software. Symmetrical devices were measured at 0 V and performed under dark conditions. For this, fitting an equivalent model similar to the one in Figure S14, Supporting Information, was used, except for the R_{rec}-CPE_{μ} element.

IMPS and IMVS: IMPS and IMVS measurements of devices were recorded under short-circuit and open-circuit conditions, respectively, with a Zahner Zennium potentiostat equipped with a frequency response analyzer module and an LED light source of 430 ± 10 nm. The DC bias illumination was adjusted to be 200 W m^{-2} and the light AC sinusoidal perturbation set to 15.5% of the DC light intensity (± 31 W m^{-2}). The frequency range was recorded from 10 kHz to 0.1 Hz.

Quenching of Y123 Dye by $[Cu(dmp)_2]^{2+}$: Mesoporous Al_2O_3 films on microscopic glass slides (prepared by spin coating Al_2O_3 paste and heating at 450 °C for 30 min) were immersed into a 0.1 mM Y123 solution in dry CH_3CN overnight inside a glovebox. After dying, films were washed with CH_3CN, dried, and placed vertically into the cuvette filled with CH_3CN, to which aliquots of $[Cu(dmp)_2]^{2+}$ or $[Cu(dmp)_2]^{2+}$-tBP solution were added. The samples were illuminated with a 440 nm pulsed laser diode (Picoquant LDH-P-C-440). The pulse energy was 8.5 pJ and the repetition rate was 20 MHz. The angle of incidence was 45° to the sample surface. The light was collected at a 90° angle to the incident laser beam and opposite the reflected laser light. The fluorescence was passed through a 500 nm dielectric long-wavelength-passing filter and a 480 mm monochromator set to 640 nm. It was recorded using a Hamamatsu R3809U-50 microchannel plate photomultiplier tube.

Steady-State Fluorescence Measurements: Y123-sensitized Al_2O_3 films on microscopic glass slides were prepared as previously described which were then cut into ≈1 × 2 cm pieces. Using 25 µm thick hot-melt Surlyn, a bare glass slide (also with dimensions of 1 × 2 cm) was attached, forming a compartment into which the CH_3CN-based solutions containing the various quenchers were filled through one of two pre-drilled holes of the glass slide inside a N_2 glovebox. Surlyn-coated aluminium foil heated to 120 °C was then used to seal the holes with the application of pressure. The fluorescence measurements were recorded on a Horiba FluoroMax-4.

Dye Regeneration Kinetics of Copper Complexes: ≈1 um thick TiO_2 films (7 × 7 mm in dimension) comprising 30 nm-sized particles were screen-printed and sintered. TiO_2 electrodes were heated with a heat gun at 500 ± 25 °C for 30 min prior to being immersed into a 3 μM solution of the dye in CH_3CN:toluene (1:1) for 24 h. The dyed TiO_2 working electrodes were fused to pre-drilled microscope glass slides (as dummy counter electrodes) with a 25 μm hot-melt Surlyn gasket, forming a compartment into which the electrolyte solutions were filled through the pre-drilled injecting holes. Electrolytes comprised 10 mM of the Cu(I) complex species dissolved in CH_3CN containing 0.1 M LiTFSI. Once filled, the injecting holes were sealed with a sheet of Surlyn-coated aluminium foil, with care taken to avoid blockage of the laser through the film.

DFT Calculations of the Reorganization Energy of Copper Complexes: Theoretical calculations for obtaining free energies and minimized ground state geometries were carried out based on DFT using Gaussian-09 rev. A. 02 package.[88] The level of theory employed was B3LYP coupled with the def2-svp basis set.[89–91] Restricted and unrestricted DFT was employed for optimizing and computing the energies of the doublet Cu(I) and singlet Cu(II) complexes. The default tight convergence criteria was used for SCF convergence. The inner sphere reorganization energy (l_i) was calculated based on previous literature.[92,93] l_i was obtained by combining the individual contributions of the reduced (l_{red}) and oxidized (l_{ox}) states. l_{ox} was calculated from the energy difference between the oxidized molecule at the minimized geometry of the reduced state and the minimized oxidized state energy. l_{red} was obtained from the energy difference between the reduced. The minimized energy structures are shown in Figure S20, Supporting Information, and the reorganization energies and differences in dihedral angles are listed in Table S7, Supporting Information.

[CCDC 2010057–2010059 contains the supplementary crystallographic data for this paper. These data can be obtained free of charge from The Cambridge Crystallographic Data Centre via www.ccdc.cam.ac.uk/data_request/cif.].

Supporting Information

Supporting Information is available from the Wiley Online Library or from the author.

Acknowledgements

S.O.F. and R.A.M. contributed equally to this work. The authors thank the Australian Centre for Advanced Photovoltaics (ACAP), the Australian Renewable Energy Agency, the Australian Research Council (ARC, LE170100235), the ARC Centre of Excellence in Exciton Science (ACEX; CE170100026), and the Swiss National Science Foundation (project P2BSP2_165366) for their financial support.

Conflict of Interest

The authors declare no conflict of interest.

Keywords

4-*tert*-butylpyridine, coordination, copper electrolyte, dye-sensitized solar cells, Lewis bases

Received: June 24, 2020
Revised: August 6, 2020

[1] D. Gielen, F. Boshell, D. Saygin, M. D. Bazilian, N. Wagner, R. Gorini, *Energy Strateg. Rev.* **2019**, *24*, 38.
[2] a) Y. Liu, Y. Cao, W. Zhang, M. Stojanovic, M. I. Dar, P. Péchy, Y. Saygili, A. Hagfeldt, S. M. Zakeeruddin, M. Grätzel, *Angew. Chem.* **2018**, *130*, 14321; b) Y. Liu, Y. Cao, W. Zhang, M. Stojanovic, M. I. Dar, P. Péchy, Y. Saygili, A. Hagfeldt, S. M. Zakeeruddin, M. Grätzel, *Angew. Chem., Int. Ed.* **2018**, *57*, 14125.
[3] M. Freitag, J. Teuscher, Y. Saygili, X. Zhang, F. Giordano, P. Liska, J. Hua, S. M. Zakeeruddin, J.-E. Moser, M. Grätzel, A. Hagfeldt, *Nat. Photonics* **2017**, *11*, 372.
[4] E. Tanaka, H. Michaels, M. Freitag, N. Robertson, *J. Mater. Chem. A* **2020**, *8*, 1279.
[5] Y. Cao, Y. Liu, S. M. Zakeeruddin, A. Hagfeldt, M. Grätzel, *Joule* **2018**, *2*, 1108.
[6] S. Yun, Y. Qin, A. R. Uhl, N. Vlachopoulos, M. Yin, D. Li, X. Han, A. Hagfeldt, *Energy Environ. Sci.* **2018**, *11*, 476.
[7] S. Venkatesan, W.-H. Lin, H. Teng, Y.-L. Lee, *ACS Appl. Mater. Interfaces* **2019**, *11*, 42780.
[8] W. Song, X. Yin, D. Liu, W. Ma, M. Zhang, X. Li, P. Cheng, C. Zhang, J. Wang, Z. L. Wang, *Nano Energy* **2019**, *65*, 103997.
[9] H. Michaels, M. Rinderle, R. Freitag, I. Benesperi, T. Edvinsson, R. Socher, A. Gagliardi, M. Freitag, *Chem. Sci.* **2020**, *11*, 2895.
[10] Y. Di, S. Jia, X. Yan, J. Liang, S. Hu, *New J. Chem.* **2020**, *44*, 791.
[11] S. S. Shin, J. H. Suk, B. J. Kang, W. Yin, S. J. Lee, J. H. Noh, T. K. Ahn, F. Rotermund, I. S. Cho, S. I. Seok, *Energy Environ. Sci.* **2019**, *12*, 958.
[12] J. Wang, Y. Cui, D. Wang, *Adv. Mater.* **2019**, *31*, 1801993.
[13] I.-Y. Jeon, M. J. Ju, J. Xu, H.-J. Choi, J.-M. Seo, M.-J. Kim, I. T. Choi, H. M. Kim, J. C. Kim, J.-J. Lee, H. K. Liu, H. K. Kim, S. Dou, L. Dai, J.-B. Baek, *Adv. Funct. Mater.* **2015**, *25*, 1170.
[14] X. Jiang, H. Li, S. Li, S. Huang, C. Zhu, L. Hou, *Chem. Eng. J.* **2018**, *334*, 419.
[15] a) X. Meng, C. Yu, X. Song, J. Iocozzia, J. Hong, M. Rager, H. Jin, S. Wang, L. Huang, J. Qiu, Z. Lin, *Angew. Chem.* **2018**, *130*, 4772; b) X. Meng, C. Yu, X. Song, J. Iocozzia, J. Hong, M. Rager, H. Jin, S. Wang, L. Huang, J. Qiu, Z. Lin, *Angew. Chem., Int. Ed.* **2018**, *57*, 4682.
[16] V. Murugadoss, J. Lin, H. Liu, X. Mai, T. Ding, Z. Guo, S. Angaiah, *Nanoscale* **2019**, *11*, 17579.
[17] J. Ou, J. Xiang, J. Liu, L. Sun, *ACS Appl. Mater. Interfaces* **2019**, *11*, 14862.
[18] G.-R. Li, X.-P. Gao, *Adv. Mater.* **2020**, *32*, 1806478.
[19] H. Song, Q. Liu, Y. Xie, *Chem. Commun.* **2018**, *54*, 1811.
[20] Y. Ren, D. Sun, Y. Cao, H. N. Tsao, Y. Yuan, S. M. Zakeeruddin, P. Wang, M. Grätzel, *J. Am. Chem. Soc.* **2018**, *140*, 2405.
[21] K. Zeng, Y. Lu, W. Tang, S. Zhao, Q. Liu, W. Zhu, H. Tian, Y. Xie, *Chem. Sci.* **2019**, *10*, 2186.
[22] Y. Kurumisawa, T. Higashino, S. Nimura, Y. Tsuji, H. Iiyama, H. Imahori, *J. Am. Chem. Soc.* **2019**, *141*, 9910.
[23] J. M. Cole, G. Pepe, O. K. Al Bahri, C. B. Cooper, *Chem. Rev.* **2019**, *119*, 7279.
[24] M. Urbani, M.-E. Ragoussi, M. K. Nazeeruddin, T. Torres, *Coord. Chem. Rev.* **2019**, *381*, 1.
[25] L. Zhang, X. Yang, W. Wang, G. G. Gurzadyan, J. Li, X. Li, J. An, Z. Yu, H. Wang, B. Cai, A. Hagfeldt, L. Sun, *ACS Energy Lett.* **2019**, *4*, 943.
[26] Y. Lu, H. Song, X. Li, H. Ågren, Q. Liu, J. Zhang, X. Zhang, Y. Xie, *ACS Appl. Mater. Interfaces* **2019**, *11*, 5046.
[27] Y. Ren, Y. Cao, D. Zhang, S. M. Zakeeruddin, A. Hagfeldt, P. Wang, M. Grätzel, *Adv. Mater.* **2020**, *32*, 2000193.
[28] K. Zeng, Y. Chen, W.-H. Zhu, H. Tian, Y. Xie, *J. Am. Chem. Soc.* **2020**, *142*, 5154.
[29] S. Galliano, F. Bella, G. Piana, G. Giacona, G. Viscardi, C. Gerbaldi, M. Grätzel, C. Barolo, *Sol. Energy* **2018**, *163*, 251.
[30] F. Bella, S. Galliano, G. Piana, G. Giacona, G. Viscardi, M. Grätzel, C. Barolo, C. Gerbaldi, *Electrochim. Acta* **2019**, *302*, 31.

[31] F. Bella, L. Porcarelli, D. Mantione, C. Gerbaldi, C. Barolo, M. Grätzel, D. Mecerreyes, *Chem. Sci.* **2020**, *11*, 1485.
[32] S. M. Feldt, E. A. Gibson, E. Gabrielsson, L. Sun, G. Boschloo, A. Hagfeldt, *J. Am. Chem. Soc.* **2010**, *132*, 16714.
[33] H. N. Tsao, C. Yi, T. Moehl, J. H. Yum, S. M. Zakeeruddin, M. K. Nazeeruddin, M. Grätzel, *ChemSusChem* **2011**, *4*, 591.
[34] T. Bessho, E. C. Constable, M. Graetzel, A. Hernandez Redondo, C. E. Housecroft, W. Kylberg, M. K. Nazeeruddin, M. Neuburger, S. Schaffner, *Chem. Commun.* **2008**, 3717.
[35] S. O. Fürer, B. Bozic-Weber, M. Neuburger, E. C. Constable, C. E. Housecroft, *RSC Adv.* **2015**, *5*, 69430.
[36] B. Bozic-Weber, E. C. Constable, C. E. Housecroft, P. Kopecky, M. Neuburger, J. A. Zampese, *Dalt. Trans.* **2011**, *40*, 12584.
[37] M. Sandroni, L. Favereau, A. Planchat, H. Akdas-Kilig, N. Szuwarski, Y. Pellegrin, E. Blart, H. Le Bozec, M. Boujtita, F. Odobel, *J. Mater. Chem. A* **2014**, *2*, 9944.
[38] H. Nusbaumer, J.-E. Moser, S. M. Zakeeruddin, M. K. Nazeeruddin, M. Grätzel, *J. Phys. Chem. B* **2001**, *105*, 10461.
[39] M. K. Kashif, J. C. Axelson, N. W. Duffy, C. M. Forsyth, C. J. Chang, J. R. Long, L. Spiccia, U. Bach, *J. Am. Chem. Soc.* **2012**, *134*, 16646.
[40] a) M. K. Kashif, M. Nippe, N. W. Duffy, C. M. Forsyth, C. J. Chang, J. R. Long, L. Spiccia, U. Bach, *Angew. Chem.* **2013**, *125*, 5637; b) M. K. Kashif, M. Nippe, N. W. Duffy, C. M. Forsyth, C. J. Chang, J. R. Long, L. Spiccia, U. Bach, *Angew. Chem., Int. Ed.* **2013**, *52*, 5527.
[41] S. O. Fürer, B. Bozic-Weber, T. Schefer, C. Wobill, E. C. Constable, C. E. Housecroft, M. Willgert, *J. Mater. Chem. A* **2016**, *4*, 12995.
[42] S. Mathew, A. Yella, P. Gao, R. Humphry-Baker, B. F. E. Curchod, N. Ashari-Astani, I. Tavernelli, U. Rothlisberger, M. K. Nazeeruddin, M. Grätzel, *Nat. Chem.* **2014**, *6*, 242.
[43] a) Z. Yao, M. Zhang, R. Li, L. Yang, Y. Qiao, P. Wang, *Angew. Chem.* **2015**, *127*, 6092; b) Z. Yao, M. Zhang, R. Li, L. Yang, Y. Qiao, P. Wang, *Angew. Chem., Int. Ed.* **2015**, *54*, 5994.
[44] a) I. R. Perera, T. Daeneke, S. Makuta, Z. Yu, Y. Tachibana, A. Mishra, P. Bäuerle, C. A. Ohlin, U. Bach, L. Spiccia, *Angew. Chem.* **2015**, *127*, 3829; b) I. R. Perera, T. Daeneke, S. Makuta, Z. Yu, Y. Tachibana, A. Mishra, P. Bäuerle, C. A. Ohlin, U. Bach, L. Spiccia, *Angew. Chem., Int. Ed.* **2015**, *54*, 3758.
[45] A. M. El-Zohry, J. Cong, M. Karlsson, L. Kloo, B. Zietz, *Dye. Pigment.* **2016**, *132*, 360.
[46] T. Daeneke, T.-H. Kwon, A. B. Holmes, N. W. Duffy, U. Bach, L. Spiccia, *Nat. Chem.* **2011**, *3*, 211.
[47] Y. Cao, Y. Saygili, A. Ummadisingu, J. Teuscher, J. Luo, N. Pellet, F. Giordano, S. M. Zakeeruddin, J.-E. Moser, M. Freitag, A. Hagfeldt, M. Grätzel, *Nat. Commun.* **2017**, *8*, 15390.
[48] M. Freitag, F. Giordano, W. Yang, M. Pazoki, Y. Hao, B. Zietz, M. Grätzel, A. Hagfeldt, G. Boschloo, *J. Phys. Chem. C* **2016**, *120*, 9595.
[49] Y. Saygili, M. Söderberg, N. Pellet, F. Giordano, Y. Cao, A. B. Munoz-García, S. M. Zakeeruddin, N. Vlachopoulos, M. Pavone, G. Boschloo, L. Kavan, J. E. Moser, M. Grätzel, A. Hagfeldt, M. Freitag, *J. Am. Chem. Soc.* **2016**, *138*, 15087.
[50] M. Freitag, Q. Daniel, M. Pazoki, K. Sveinbjornsson, J. Zhang, L. Sun, A. Hagfeldt, G. Boschloo, *Energy Environ. Sci.* **2015**, *8*, 2634.
[51] S. Hattori, Y. Wada, S. Yanagida, S. Fukuzumi, *J. Am. Chem. Soc.* **2005**, *127*, 9648.
[52] C. Förster, K. Heinze, *Chem. Soc. Rev.* **2020**, *49*, 1057.
[53] E. T. Adman, *Adv. Protein Chem.* **1991**, *41*, 145.
[54] Y. Bai, Q. Yu, N. Cai, Y. Wang, M. Zhang, P. Wang, *Chem. Commun.* **2011**, *47*, 4376.
[55] W. Zhang, Y. Wu, H. W. Bahng, Y. Cao, C. Yi, Y. Saygili, J. Luo, Y. Liu, L. Kavan, J.-E. Moser, A. Hagfeldt, H. Tian, S. M. Zakeeruddin, W.-H. Zhu, M. Grätzel, *Energy Environ. Sci.* **2018**, *11*, 1779.
[56] G. Boschloo, L. Häggman, A. Hagfeldt, *J. Phys. Chem. B* **2006**, *110*, 13144.
[57] M. T. Miller, P. K. Gantzel, T. B. Karpishin, *Inorg. Chem.* **1998**, *37*, 2285.
[58] L. N. Ashbrook, C. M. Elliott, *J. Phys. Chem. C* **2013**, *117*, 3853.
[59] L. Kavan, Y. Saygili, M. Freitag, S. M. Zakeeruddin, A. Hagfeldt, M. Grätzel, *Electrochim. Acta* **2017**, *227*, 194.
[60] Y. Wang, T. W. Hamann, *Chem. Commun.* **2018**, *54*,12361.
[61] W. L. Hoffeditz, M. J. Katz, P. Deria, G. E. Cutsail III, M. J. Pellin, O. K. Farha, J. T. Hupp, *J. Phys. Chem. C* **2016**, *120*, 3731.
[62] Y. Saygili, M. Stojanovic, H. Michaels, J. Tiepelt, J. Teuscher, A. Massaro, M. Pavone, F. Giordano, S. M. Zakeeruddin, G. Boschloo, J. Moser, M. Grätzel, A. B. Muñoz-García, A. Hagfeldt, M. Freitag, *ACS Appl. Energy Mater.* **2018**, *1*, 4950.
[63] K. Kannankutty, C. C. Chen, V. S. Nguyen, Y. C. Lin, H. H. Chou, C. Y. Yeh, T. C. Wei, *ACS Appl. Mater. Interfaces* **2020**, *12*, 5812.
[64] B. Murphy, *Coord. Chem. Rev.* **2003**, *243*, 237.
[65] L. X. Chen, G. B. Shaw, I. Novozhilova, T. Liu, G. Jennings, K. Attenkofer, G. J. Meyer, P. Coppens, *J. Am. Chem. Soc.* **2003**, *125*, 7022.
[66] C. Zhang, J. Dai, Z. Huo, X. Pan, L. Hu, F. Kong, Y. Huang, Y. Sui, X. Fang, K. Wang, S. Dai, *Electrochim. Acta* **2008**, *53*, 5503.
[67] T. Stergiopoulos, E. Rozi, C. Karagianni, P. Falaras, *Nanoscale Res. Lett.* **2011**, *6*, 307.
[68] H. Ellis, R. Jiang, S. Ye, A. Hagfeldt, G. Boschloo, *Phys. Chem. Chem. Phys.* **2016**, *18*, 8419.
[69] V. Leandri, Q. Daniel, H. Chen, L. Sun, J. M. Gardner, L. Kloo, *Inorg. Chem.* **2018**, *57*, 4556.
[70] D. Tran, B. W. Skelton, A. H. White, L. E. Laverman, P. C. Ford, *Inorg. Chem.* **1998**, *37*, 2505.
[71] V. V. Pavlishchuk, A. W. Addison, *Inorganica Chim. Acta* **2000**, *298*, 97.
[72] T. C. Richards, W. E. Geiger, *J. Am. Chem. Soc.* **1994**, *116*, 2028.
[73] A. M. Bond, R. Colton, *Coord. Chem. Rev.* **1997**, *166*, 161.
[74] M. M. Bernardo, P. V. Robandt, R. R. Schroeder, D. B. Rorabacher, *J. Am. Chem. Soc.* **1989**, *111*, 1224.
[75] G. Redmond, D. Fitzmaurice, *J. Phys. Chem.* **1993**, *97*, 1426.
[76] G. Schlichthörl, S. Y. Huang, J. Sprague, A. J. Frank, *J. Phys. Chem. B* **1997**, *101*, 8141.
[77] M. K. Nazeeruddin, A. Kay, I. Rodicio, R. Humphry-Baker, E. Mueller, P. Liska, N. Vlachopoulos, M. Graetzel, *J. Am. Chem. Soc.* **1993**, *115*, 6382.
[78] M. J. Katz, M. J. D. Vermeer, O. K. Farha, M. J. Pellin, J. T. Hupp, *Langmuir* **2013**, *29*, 806.
[79] S. A. Haque, Y. Tachibana, R. L. Willis, J. E. Moser, M. Grätzel, D. R. Klug, J. R. Durrant, *J. Phys. Chem. B* **2000**, *104*, 538.
[80] M. K. Kashif, R. A. Milhuisen, M. Nippe, J. Hellerstedt, D. Z. Zee, N. W. Duffy, B. Halstead, F. De Angelis, S. Fantacci, M. S. Fuhrer, C. J. Chang, Y.-B. Cheng, J. R. Long, L. Spiccia, U. Bach, *Adv. Energy Mater.* **2016**, *6*, 1600874.
[81] F. Fabregat-Santiago, G. Garcia-Belmonte, I. Mora-Seró, J. Bisquert, *Phys. Chem. Chem. Phys.* **2011**, *13*, 9083.
[82] F. Fabregat-Santiago, J. Bisquert, E. Palomares, L. Otero, D. Kuang, S. M. Zakeeruddin, M. Grätzel, *J. Phys. Chem. C* **2007**, *111*, 6550.
[83] A. Hagfeldt, G. Boschloo, L. Sun, L. Kloo, H. Pettersson, *Chem. Rev.* **2010**, *110*, 6595.
[84] S. R. Raga, E. M. Barea, F. Fabregat-Santiago, *J. Phys. Chem. Lett.* **2012**, *3*, 1629.
[85] A. Yella, H.-W. Lee, H. N. Tsao, C. Yi, a. K. Chandiran, M. K. Nazeeruddin, E. W.-G. Diau, C.-Y. Yeh, S. M. Zakeeruddin, M. Gratzel, *Science* **2011**, *334*, 629.
[86] H. Ellis, N. Vlachopoulos, L. Häggman, C. Perruchot, M. Jouini, G. Boschloo, A. Hagfeldt, *Electrochim. Acta* **2013**, *107*, 45.
[87] C. O. Dietrick-Buchecker, P. A. Marnot, J. P. Sauvage, *Tetrahedron Lett.* **1982**, *23*, 5291.
[88] M. J. Frisch, G. W. Trucks, H. B. Schlegel, G. E. Scuseria, M. A. Robb, J. R. Cheeseman, G. Scalmani, V. Barone, B. Mennucci,

G. A. Petersson, H. Nakatsuji, M. Caricato, X. Li, H. P. Hratchian, A. F. Izmaylov, J. Bloino, G. Zheng, J. L. Sonnenberg, M. Hada, M. Ehara, K. Toyota, R. Fukuda, J. Hasegawa, M. Ishida, T. Nakajima, Y. Honda, O. Kitao, H. Nakai, T. Vreven, J. A. Montgomery Jr., et al., Gaussian 09, Revision A.02, Gaussian Inc., Wallingford, CT **2009**.

[89] C. Lee, W. Yang, R. G. Parr, *Phys. Rev. B* **1988**, *37*, 785.

[90] A. D. Becke, *Phys. Rev. A* **1988**, *38*, 3098.

[91] F. Weigend, R. Ahlrichs, *Phys. Chem. Chem. Phys.* **2005**, *7*, 3297.

[92] M. H. M. Olsson, U. Ryde, *J. Am. Chem. Soc.* **2001**, *123*, 7866.

[93] M. Gennari, J. Pécaut, M. N. Collomb, C. Duboc, *Dalt. Trans.* **2012**, *41*, 3130.